Journal of the Korean Society of Agricultural Engineers
Vol. 55, No. 5, pp. 59~69, September, 2013
DOI:http://dx.doi.org/10.5389/KSAE.2013.55.5.059

ISSN 1738-3692
eISSN 2093-7709

Liquefaction Analysis at Multi-Layered Ground Considering Viscoplastic Effect of Clay

점성토의 점소성 효과를 고려한 다층지반의 액상화 해석

Yoon, Yong-Sun* · **Lee, Jae-Deuk*** · **Kim, Yong-Seong****,†

윤용선 · **이재득** · **김용성**

ABSTRACT

본 연구에서는 동적 점탄-점소성 구성식에 기초한 다층지반의 1차원 액상화 해석을 수행하였다. 일본 고베 포트아일랜드에서 발생한 1995 Hyogoken Nanbu 지진에 대하여 지반 모델링을 하였으며, 사질토 지반에는 탄소성 모델을, 점성토 지반에는 점탄-점소성 모델 및 탄-점소성 모델을 각각 적용하였다. 본 연구 결과, 모델 지반의 경우 지표 10 m 아래를 전후하여 액상화가 발생하였으며 액상화가 발생한 지반을 통과하는 지진파는 감쇠특성을 나타내고 이 때 전단변형률을 크게 증가시켰다. 또한, 대변형률 영역에서의 점성토의 동적거동 해석에서는 점소성 거동특성이 지배적이므로 점소성 모델의 적용이 중요함을 알 수 있었다. 한편 동적 점탄-점소성 구성모델은 대변형률 영역에서 점성토의 소성변형을 유발하는 대형 지진 발생시 점성토의 증폭 및 감쇠특성 분석에 적용 가능한 모델임을 확인하였다.

Keywords: Clay, dynamic analysis, viscoplastic, constitutive model, earthquake

I. INTRODUCTION

Until now, viscoelastic constitutive models have been used to simulate the behavior of materials such as polymer, concrete, metal and soil. Mainly, linear viscoelastic model such as Maxwell model, Voigt model and three parameter model have been used for the analysis of viscoelastic behavior. Kondner (1965) and Hori (1974) reported that three parameter model which consists of a free spring as the instantaneous elasticity, and the Voigt element, in parallel, as the retardation elasticity can explain approximately the dynamic behavior of clay. Moreover, Murayama and Shibata (1966) proved the time dependency of clay in high frequency region by considering the distribution of relaxation time (Oka et al., 2001).

Generally, if strain level is low, the time dependent behavior of clay can be expressed by a viscoelastic model, but if strain level is large, the viscoplastic model will be needed for the effect of high plasticity. Therefore, when one considers developing constitutive models for clay, in the wide strain level, a viscoelastic- viscoplastic approach is preferable. The linear viscoelastic approach is valid for the behavior in the range of small strain, while viscoplastic modeling of soils is useful in the range of large strain including failure (Kim, 2001).

The constitutive model has been incorporated into a coupled finite element-finite difference (FEM-FDM) numerical method for the liquefaction analysis of fluid-saturated ground. The applicability of the proposed numerical method has been verified in the past studies (Yashima et al., 1995; Taguchi et al., 1996; Oka et al., 1996, 1997).

Meanwhile, the ground motions in the near-source region during the 1995 Hyogoken Nanbu Earthquake were so strong that soft ground layers forced to behave nonlinearly. Non-linear ground motion amplification owing to the input motion level at bedrock is one of the important topics to understand various geomaterials behavior. The extremely valuable borehole records at Port Island were obtained during the 1995 Hyogoken Nanbu Earthquake (Kim et al., 2005; Kim, 2006)

In the present study, the non-linear ground motion ampli-

* 강원대학교 대학원 지역건설공학과
** 강원대학교 지역건설공학과 부교수
† Corresponding author Tel.: +82-33-250-6463
Fax: +82-33-251-6463
E-mail: yskim2@kangwon.ac.kr
2013년 8월 19일 투고
2013년 9월 5일 심사완료
2013년 9월 10일 게재확정

fication at the soft reclaimed ground is discussed using the cyclic viscoelastic-viscoplastic model for clay. Through the seismic response analysis for main shock at Port Island, the effect of clay layer laying beneath liquefiable sand layer to dynamic properties of the whole sand-clay layered ground is considered, in particular during large earthquake. Moreover, comparison of measured records with numerical simulation results is made with focus on time-dependent characteristics and the dissipation in excess pore water pressure after the main event.

II. A VISCOELASTIC-VISCOPLASTIC CONSTITUTIVE MODEL FOR CLAY

1. A Viscoelastic-Viscoplastic Constitutive Model

A cyclic viscoelastic-viscoplastic constitutive model is formulated by incorporating a three-parameter viscoelastic component into an elasto-viscoplastic constitutive model based on non-linear kinematic hardening rule, which was proposed by Oka et al. (1992). The three-parameter viscoelastic model, which combines a Voigt viscoelastic model and a linear elastic spring in series, has been used to describe a time dependent behavior of clay for the range of low level strain by several researchers (i.e. Hori, 1974; Di Benedetto and Tatsuoka, 1997; Oka et al., 2001).

In viscoelastic region, the three parameter model with Voigt element and elastic spring is adopted and the behavior of viscoelastic materials in uni-axial stress closely resembles that of models built from discrete elastic and viscous elements (Kim, 2001). Therefore, the viscoelastic deviatoric strain rate tensor consists of elastic and viscoelastic Voigt components as

$$\dot{e}_{ij}^{ve} = \dot{e}_{ij}^{e} + \dot{e}_{ij}^{vev} = \frac{1}{2G_1}\dot{S}_{ij} + \frac{1}{\mu}\left(S_{ij} - 2G_2 e_{ij}^{vev}\right) \tag{1}$$

The stress rate tensor is given by

$$\dot{S}_{ij} = 2G_1\left\{\dot{e}_{ij} - \frac{1}{\mu}\left(S_{ij} - 2G_2 e_{ij}^{ve}\right) - \dot{e}_{ij}^{vp}\right\} \tag{2}$$

Considering the non-linear kinematic hardening rule, static yield functions are given as follows (Oka et al., 2001). For changes in the stress ratio, the static yield function used is

$$f_{y1} = \left\{\left(\eta_{ij}^{*} - \chi_{ij}^{*}\right)\left(\eta_{ij}^{*} - \chi_{ij}^{*}\right)\right\}^{1/2} - R_{D1} = 0 \tag{3}$$

The evolution equation for kinematic hardening parameter is given by

$$d\chi_{ij}^{*} = B^{*}\left(A^{*} de_{ij}^{vp} - \chi_{ij}^{*} d\gamma^{vp}\right) \tag{4}$$

$$B^{*} = B_s + (B_0 - B_s)\exp\left(-B_l \gamma^{vp}\right) \tag{5}$$

The viscoplastic strain rate tensor corresponding to is assumed to be given by

$$\dot{\varepsilon}_{ij}^{vp} = < \Phi_{ijkl}(F) > \frac{\partial f^{vp}}{\partial \sigma'_{ij}} \tag{6}$$

$$\frac{\partial f^{vp}}{\partial \sigma'_{m}} = \frac{1}{\sigma'_{m}}\left\{\tilde{M}^{*} - \frac{\eta_{mn}^{*}\left(\eta_{mn}^{*} - \chi_{mn}^{*}\right)}{\left\{\left(\eta_{ij}^{*} - \chi_{mn}^{*}\right)\left(\eta_{ij}^{*} - \chi_{mn}^{*}\right)\right\}^{1/2}}\right\} \tag{7}$$

By using the Eqs. (6) and (7), viscoplastic deviator strain increment tensor and viscoplastic volumetric strain increment can be indicated as

$$de_{ij}^{vp} = C_1 \frac{< \Phi'(F) >}{\sigma'_{m}} \frac{\eta_{ij}^{*} - \chi_{ij}^{*}}{\left\{\left(\eta_{st}^{*} - \chi_{st}^{*}\right)\left(\eta_{st}^{*} - \chi_{st}^{*}\right)\right\}^{1/2}} \tag{8}$$

$$du^{vp} = d\varepsilon_{kk}^{vp} = C_2 \frac{< \Phi'(F) >}{\sigma'_{m}} \left\{\tilde{M}^{*} - \frac{\eta_{mn}^{*}\left(\eta_{mn}^{*} - \chi_{mn}^{*}\right)}{\left\{\left(\eta_{ij}^{*} - \chi_{mn}^{*}\right)\left(\eta_{ij}^{*} - \chi_{mn}^{*}\right)\right\}^{1/2}}\right\} \tag{9}$$

So, a general description of the cyclic viscoelastic-viscoplastic model for clay is given by

$$\begin{aligned}\dot{\varepsilon}_{ij} = {} & \frac{1}{2G_1}\dot{S}_{ij} + \frac{1}{\mu}\left(S_{ij} - 2G_2 e_{ij}^{vp}\right) + \frac{\kappa}{3(1+e)}\frac{\dot{\sigma}'_{m}}{\sigma'_{m}}\delta_{ij} \\ & + C_1 \frac{< \Phi'(F) >}{\sigma'_{m}} \frac{\left(\eta_{ij}^{*} - \chi_{ij}^{*}\right)}{\bar{\eta}_{x}^{*}} \\ & + C_2 \frac{< \Phi'(F) >}{\sigma'_{m}} \left\{\tilde{M}^{*} - \frac{\eta_{mn}^{*}\left(\eta_{mn}^{*} - \chi_{mn}^{*}\right)}{\bar{\eta}_{x}^{*}}\right\}\frac{1}{3}\delta_{ij}\end{aligned} \tag{10}$$

III. VISCOPLASTIC CHARACTERISTICS IN THE LARGE STRAIN RANGE

The effects of several parameters related to viscoplastic characteristics of clay are studied. Figs. 1～3 show the effect of varying viscoplastic parameter Bs. Attention is focused on the shape of the stress-strain curves in Figs. 1～3 (a) with variations in the viscoplastic parameter B* in Figs. 1～3 (c). Rapid reduction of the viscoplastic parameter B* gives rise to large amounts of increasing strain for each

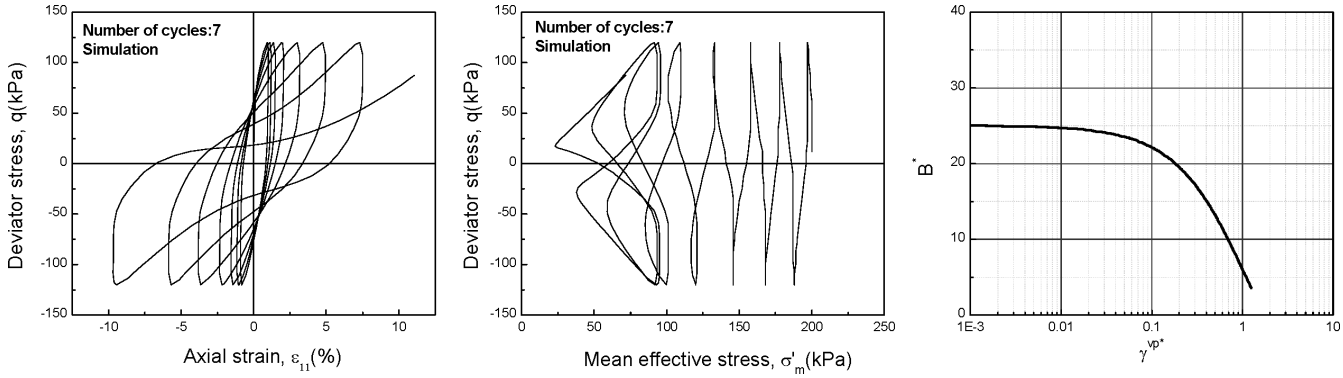

(a) Deviator stress vs. axial strain (b) Deviator stress vs. effective stress (c) γ^{vp*} vs. B^*

Fig. 1 The effects of viscoplastic parameters B^* (B_0: 25, B_s: 0.5, B_t: 1)

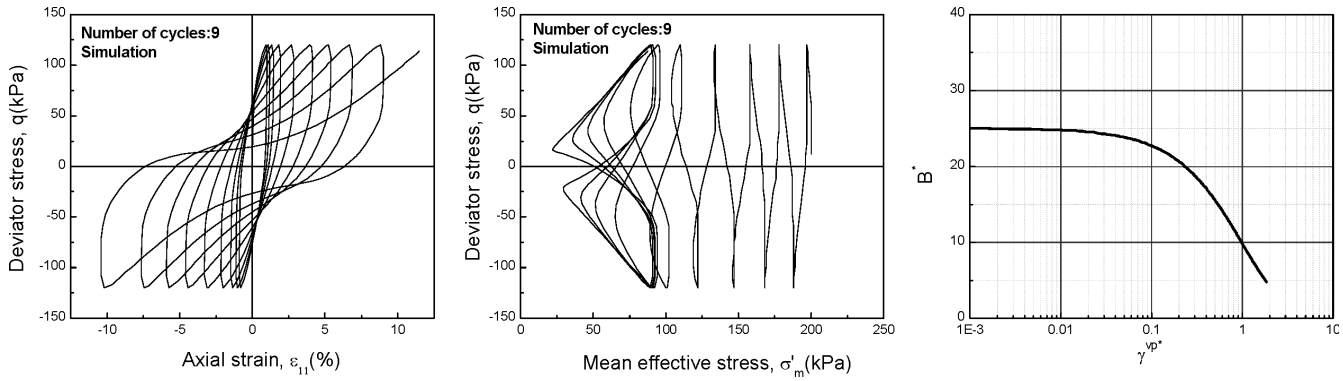

(a) Deviator stress vs. axial strain (b) Deviator stress vs. effective stress (c) γ^{vp*} vs. B^*

Fig. 2 The effects of viscoplastic parameters B^* (B_0: 25, B_s: 1, B_t :1)

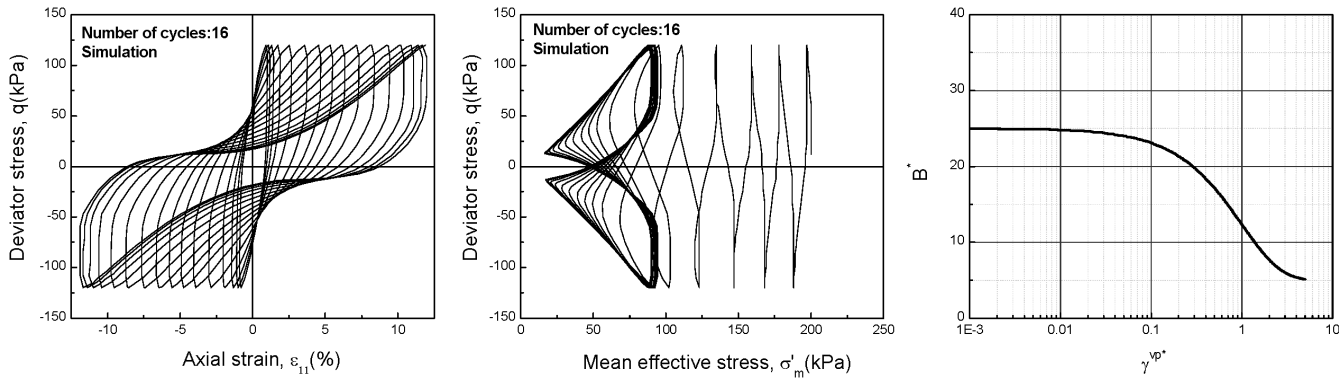

(a) Deviator stress vs. axial strain (b) Deviator stress vs. effective stress (c) γ^{vp*} vs. B^*

Fig. 3 The effects of viscoplastic parameters B^* (B_0: 25, B_s: 5, B_t :1)

cycle.

The effect of parameter Bs gives similar trend as shown in Fig. 4～6. The parameters B0, Bs and Bt control the viscoplastic parameter B*. At 1.0 of the second invariant of the viscoplastic deviatoric strain γvp^*, Fig. 4 (c) shows lower value of the viscoplastic parameter B* with larger viscoplastic behavior as shown in Fig. 4 (a) while Fig. 6 indicates larger value of that with lower viscoplastic behavior than Fig. 4.

Figs. 7～9 show effect of viscoplastic parameters C01

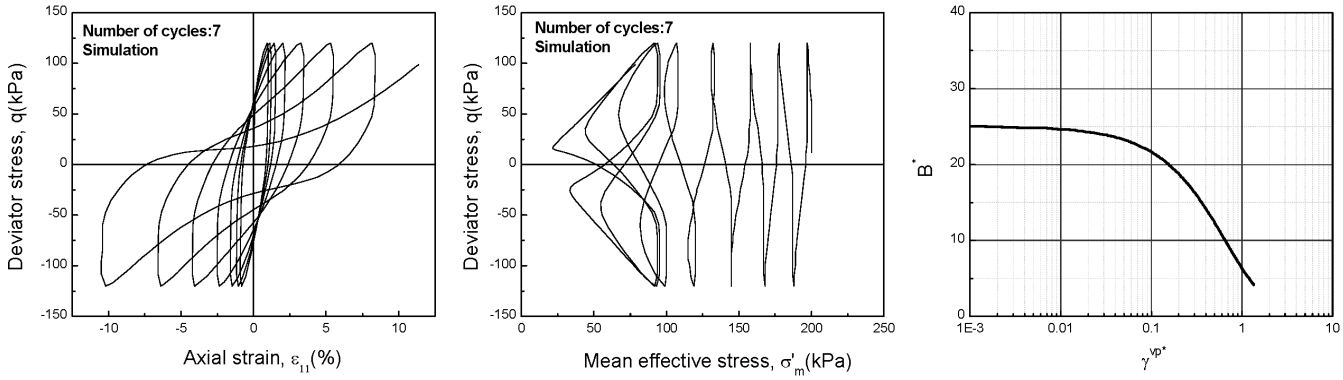

(a) Deviator stress vs. axial strain (b) Deviator stress vs. effective stress (c) γ^{vp*} vs. B^*

Fig. 4 The effects of viscoplastic parameters B^* (B_0: 25, B_s: 1, B_t: 1.5)

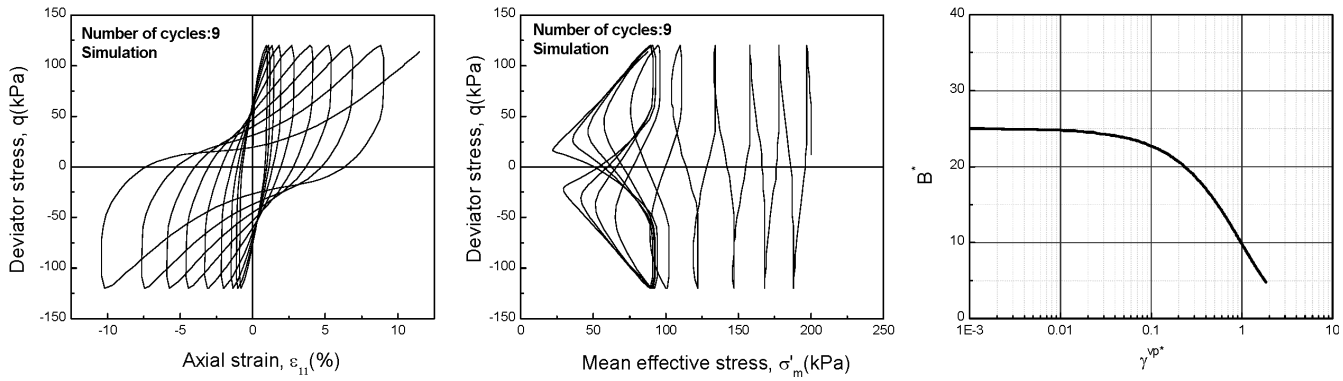

(a) Deviator stress vs. axial strain (b) Deviator stress vs. effective stress (c) γ^{vp*} vs. B^*

Fig. 5 The effects of viscoplastic parameters B^* (B_0: 25, B_s: 1, B_t: 1)

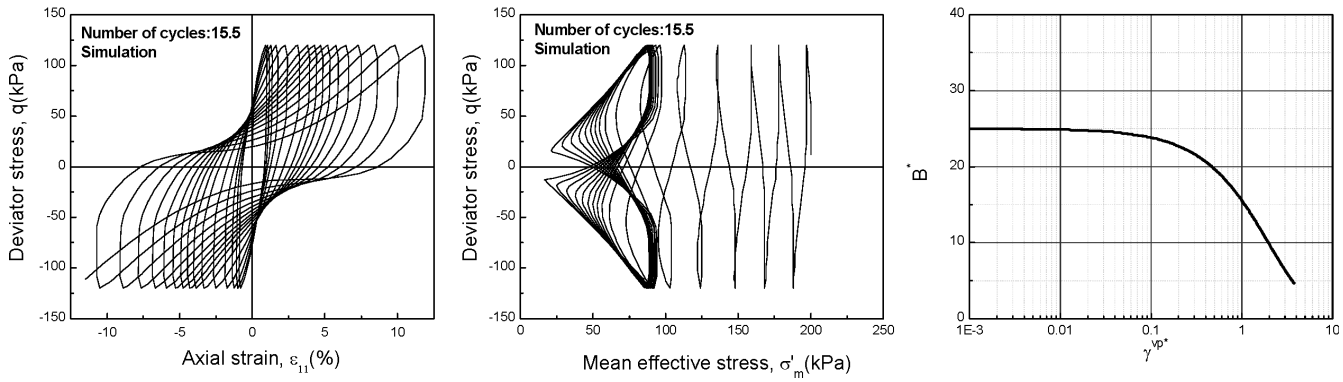

(a) Deviator stress vs. axial strain (b) Deviator stress vs. effective stress (c) γ^{vp*} vs. B^*

Fig. 6 The effects of viscoplastic parameters B^* (B_0: 25, B_s: 1, B_t: 0.5)

and C02. If these viscoplastic parameters are large, the clay displays more viscoplastic behavior in Fig. 7. On the other hand, the use of small viscoplastic parameters in stress-strain relations gives large hysteresis loop, see Fig. 9. Although in the usual case of cyclic triaxial test, 10 % of double amplitude axial strain is adopted for number of cycles, to examine the model behavior at large strain levels, the analysis are performed until 10 % of single amplitude axial strain in this study. Therefore the number of cycle is set based on the 10 % of single amplitude axial strain.

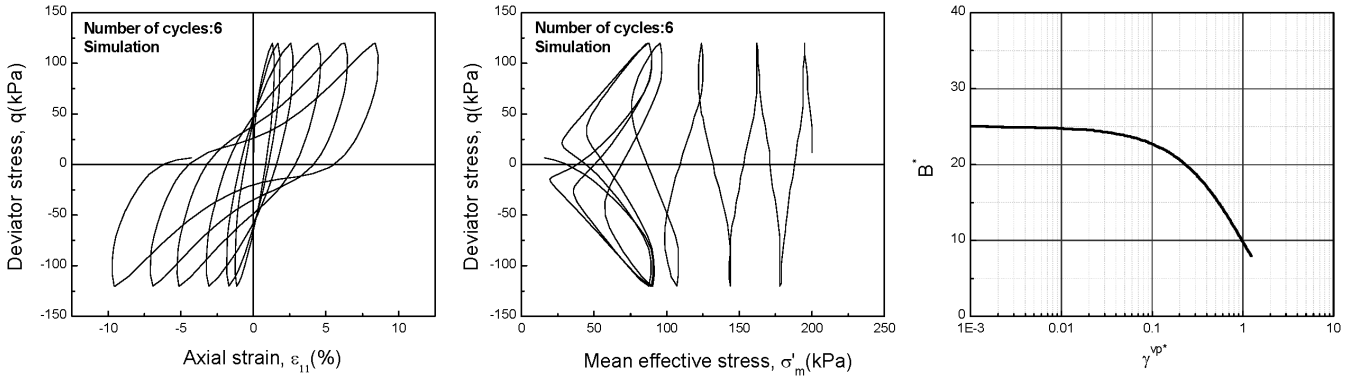

(a) Deviator stress vs. axial strain (b) Deviator stress vs. effective stress (c) γ^{vp*} vs. B^*

Fig. 7 The effects of viscoplastic parameters C01: 2.0E-05 and C02: 1.7E-09

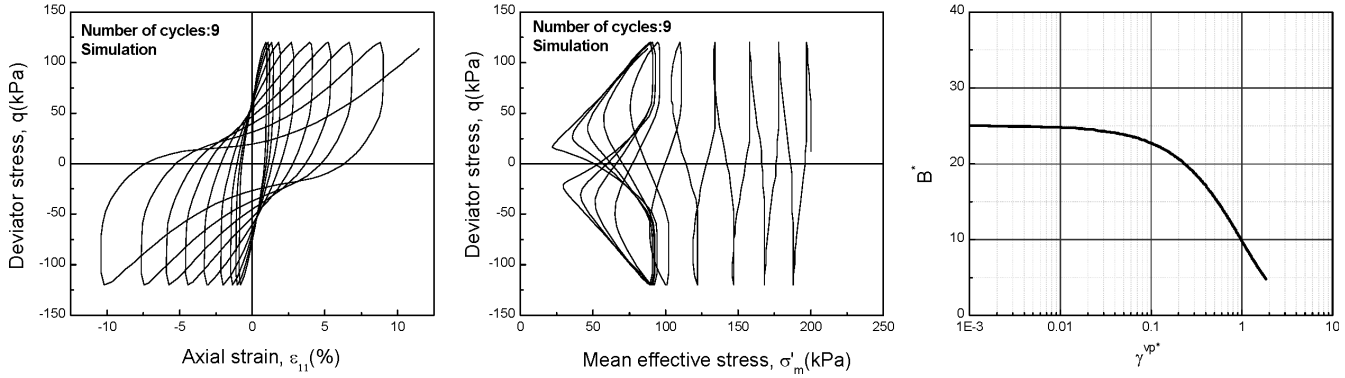

(a) Deviator stress vs. axial strain (b) Deviator stress vs. effective stress (c) γ^{vp*} vs. B^*

Fig. 8 The effects of viscoplastic parameters C01: 2.0E-06 and C02: 1.7E-10

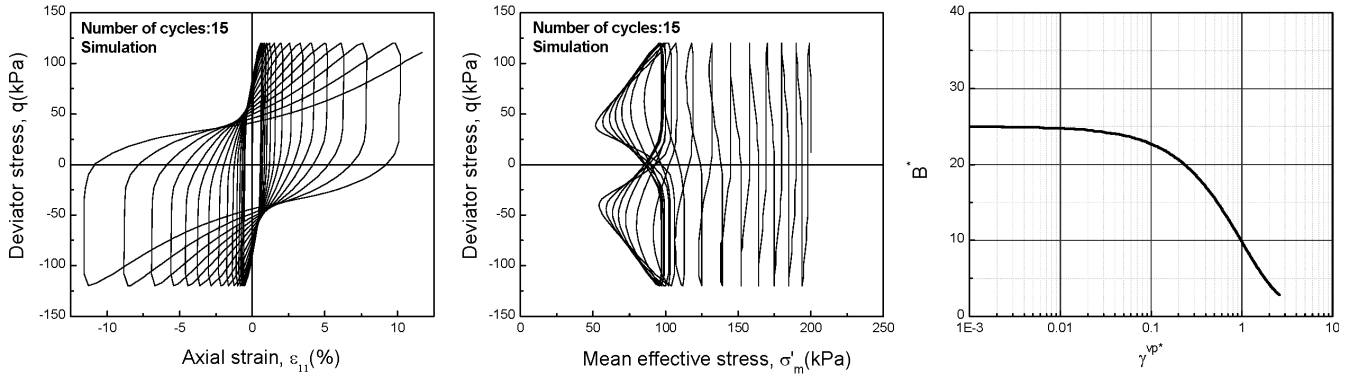

(a) Deviator stress vs. axial strain (b) Deviator stress vs. effective stress (c) γ^{vp*} vs. B^*

Fig. 9 The effects of viscoplastic parameters C01: 2.0E-07 and C02: 1.7E-11

IV. LIQUEFACTION ANALYSIS OF MULTI-LAYERED GROUND

1. Ground Condition

The 1995 Hyogoken Nanbu Earthquake (M=7.2), commonly referred to as the Kobe earthquake, was one of the most devastating earthquakes ever hit Japan. Port Island is an artificial island due south of Kobe central business district. It has been observed that Port Island was extensively liquefied during the main event. Because liquefaction only occurs in saturated soil, its effects are most commonly observed in low-lying areas near bodies of water such as rivers, lakes, bays, and oceans.

Fig. 10 shows the locations and layout of array systems of one borehole station as well as their soil profile and velocity structures. An observation system consists of four acceleration sensors and the acceleration sensors are installed at a depth of GL.0.0 m, −16.0 m, −32.0 m, and −83.0 m as shown in Fig. 10.

The first phase reclamation work of Port Island was finished in 1981, then the second phase reclamation work was started 1986 and finished 1996. A decomposed granite soil known as 'Masado' was used in the reclamation area of

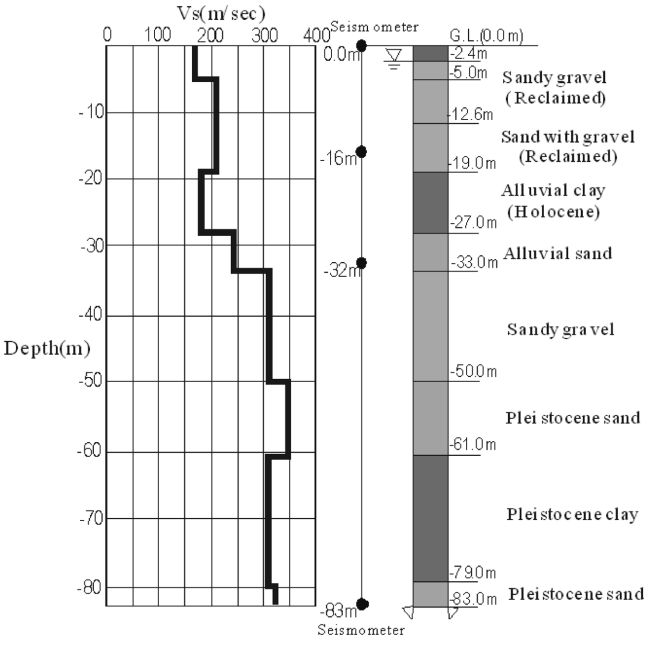

Fig. 10 Soil profile & Vs distribution

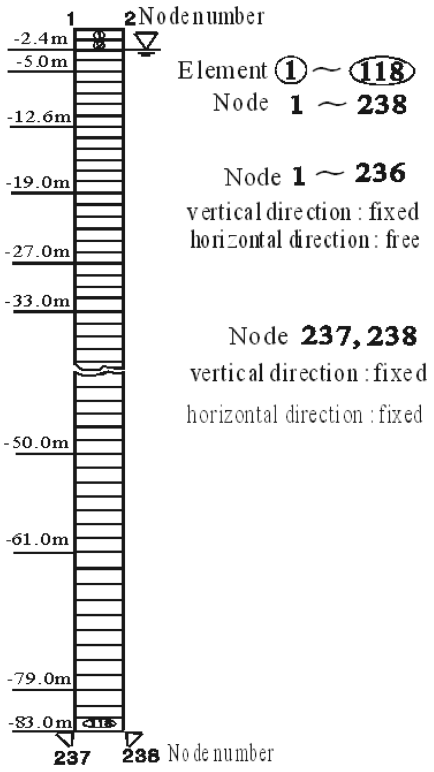

Fig. 11 FEM meshes

Port Island. At the northern areas near water front, Masado was used for reclamation. At Port Island, the velocity structure has been investigated after the earthquake using a suspension-type investigator. As shown in Fig. 1, the shear wave velocity of the alluvial clay at Port Island is 180 m/s (investigated in May 1995).

Fig. 11 shows finite element meshes of the ground model at Port Island used in the analysis. The total depth of FEM mesh at Port Island is 83m and the width is 0.5 m, and the whole area is divided into 118 rectangular elements for finite element analysis. Displacements at the bottom nodes of soil column are fixed in both horizontal and vertical directions and other nodes are fixed in the vertical direction, but are free in the horizontal direction and equi-horizontal displacement is assumed. Drainage is only allowed at the surface. Moreover plane strain condition is considered in the present study.

2. Liquefaction Analysis at Port Island

The numerical simulation of the earthquake records

Table 1 Soil parameters used in the analysis at Port Island

Parameters \ Depth (-m) / Soil type	0-2.4 Sand	2.4-5 Sand	5-12.6 Sand	12.6-19 Sand	19-27 Clay	27-33 Sand	33-50 Sand	50-61 Sand	61-79 Clay	79-83 Sand
Compressional wave Vp (m/s)	260	330	780	1480	1180	1330	1530	1610	1610	2000
Shear wave Vs (m/s)	170	170	210	210	180	245	305	350	303	320
Viscous parameters μ (kPa · s)	0	0	0	0	5.0E+03	0	0	0	5.0E+03	320
Viscoplastic parameter m'	-	-	-	-	2.0E-07	-	-	-	1.0E-09	-
Viscoplastic parameter C_{01} (1/s)	-	-	-	-	2.0E-09	-	-	-	1.0E-11	-
Viscoplastic parameter C_{02} (1/s)	-	-	-	-	20	-	-	-	20	-
Viscoplastic parameter B_0	100	100	70	500	50	1000	2000	3000	100	5000
Viscoplastic parameter B_s	1	1	1	1	1	1	1	1	1	1
Viscoplastic parameter B_t	1	1	1	1	1	1	1	1	1	1
Stress ratio at maximum compression M_m^*	0.71	0.71	0.75	0.75	0.74	0.91	1.16	1.16	0.99	1.16
Stress ratio at failure state M_f^*	1.01	1.01	1.05	1.05	1.24	1.21	1.41	1.57	1.24	1.57
Compression index λ	0.03	0.3	0.03	0.3	0.39	0.02	0.02	0.02	0.34	0.03
Swelling index κ	0.00026	0.00027	0.00054	0.00072	0.05	0.00133	0.0011	0.00114	0.00261	0.00203
Poisson's ratio υ	0.25	0.25	0.25	0.25	0.488	0.25	0.25	0.25	0.3	0.25
Initial void ratio e_0	0.6	0.6	0.6	0.6	1.5	0.6	0.5	0.5	1.2	0.5

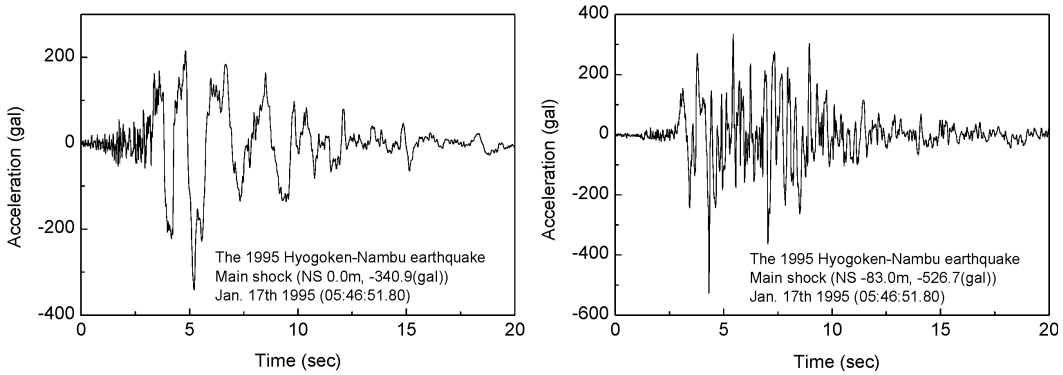

(a) GL.0.0 m (b) GL.－83.0 m

Fig. 12 Observed acceleration record at Port Island

obtained at instrumented site at Port Island, Kobe, was performed by the computer program LIQCA-2D (VE-VP). In the analysis, horizontal shaking was applied to the soil layers composed of sand and clay. Here, importance of taking into account the clay behavior to the liquefaction analysis in multi-layered ground is emphasized.

The viscoelastic-viscoplastic constitutive model was used to simulate the cohesive soil behavior, and all the initial state and soil parameters were obtained using the previous research works (Yashima et al., 1995; Taguchi et al., 1996; Oka et al., 1996, 1997). Table 1 shows the parameters used in the analysis.

Fig. 12 shows the obtained record of earthquake acceleration (GL.0.0 m), which is NS component of horizontal direction and the input motion (GL.－83 m). From the specification for the instrumented site at Port Island, Kobe, accelerometers were placed at four different depths. NS directional components of acceleration at the three different depths, for example GL.0.0 m, －16 m and －32 m, were reported. In the present analysis, all the predictions and comparisons were made at the three different depths in NS directions.

Figs. 13～15 show the numerical results in which shear wave velocity Vs of alluvial clay layer at Port Island is 180 m/s referenced from Fig. 10. Fig. 13 shows obtained records and evaluated accelerations of the main shock occurred on

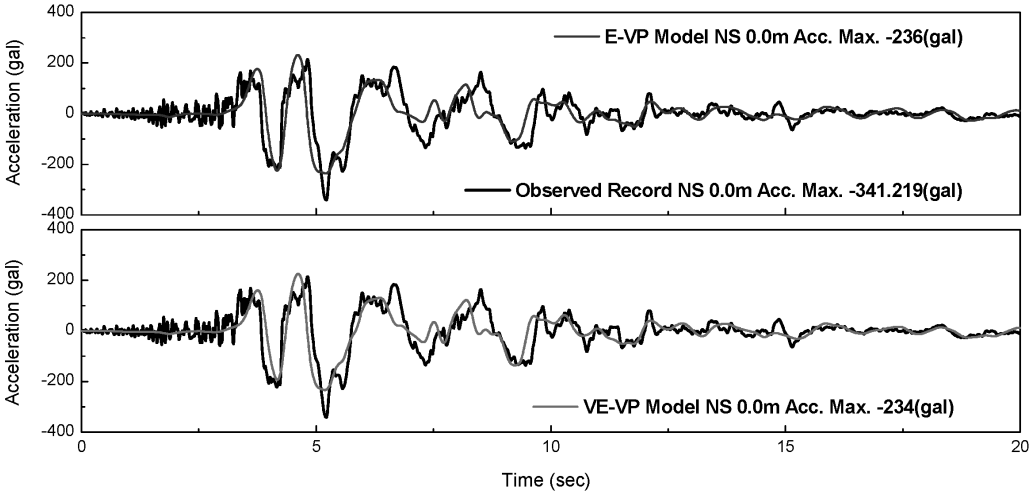

(a) 0.0 m sand layer

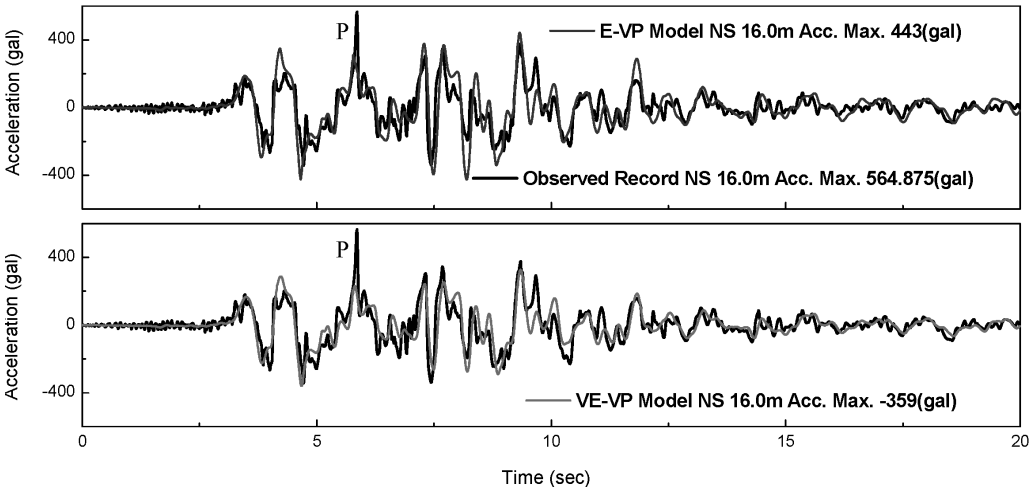

(b) 16.0 m sand layer

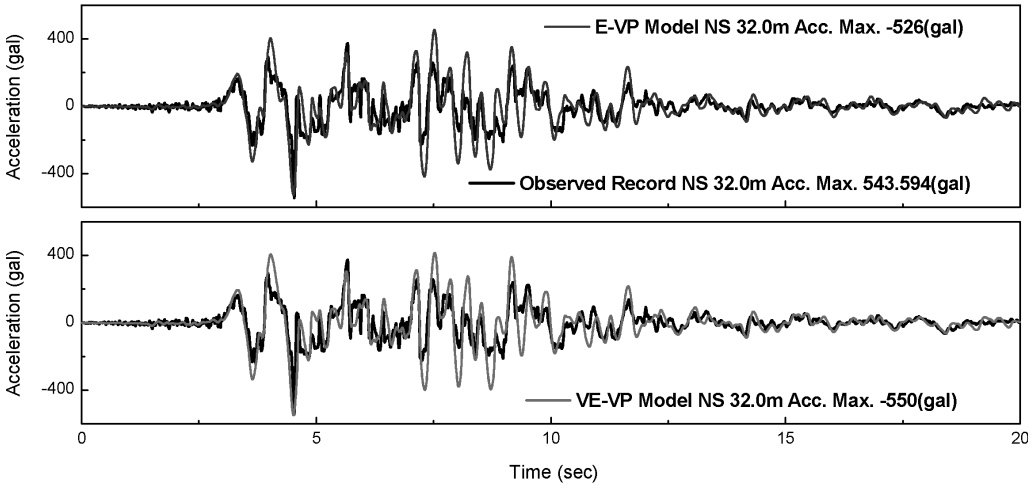

(c) 32.0 m sand layer

Fig. 13 Observed record vs. simulation results with E-VP model and VE-VP model

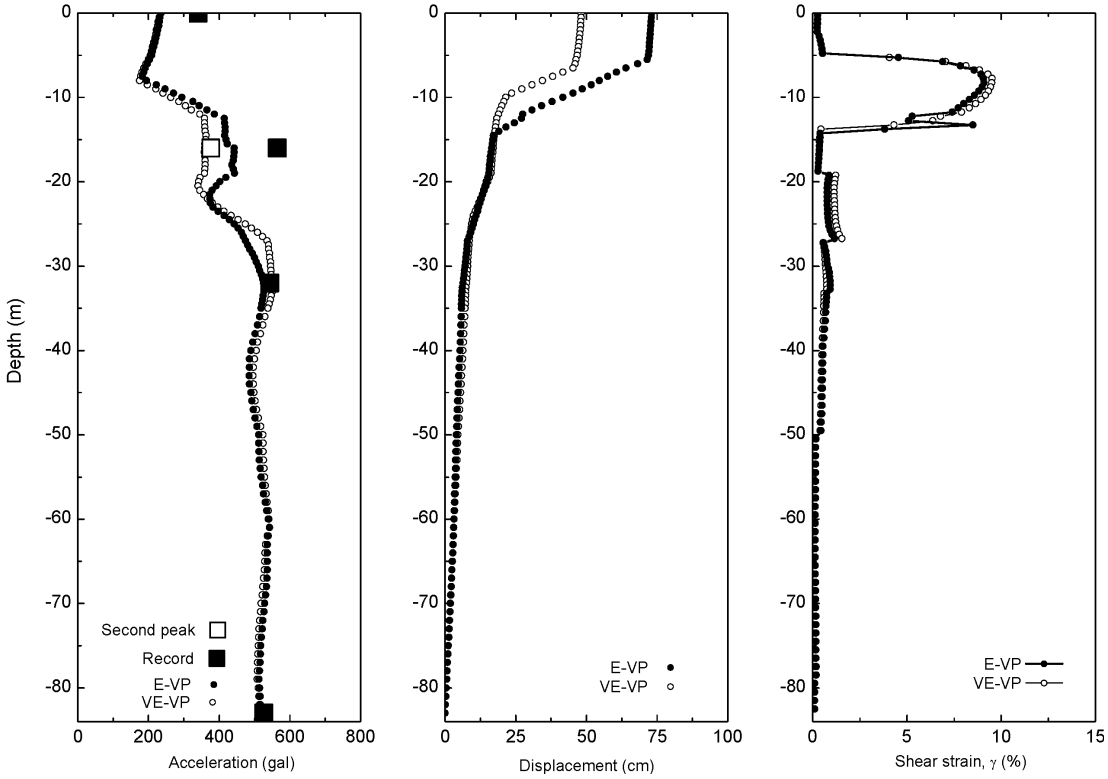

(a) Acceleration (b) Displacement (c) Shear strain

Fig. 14 Maximum value distribution of seismic response analysis at Port Island

17th Jan. 1995 at Port Island. Black line shows obtained record and the upper part at each figures displays the numerical results by an elasto-viscoplastic model while the lower part shows the numerical results by a viscoelastic-viscoplastic model. As shown in Table 1, the viscous coefficient of 5.0×10^3 kPa · sec is used in the viscoelastic-viscoplastic approach. Almost the same results between these two models are obtained in Figs. 13 (a) and (c). However, these two models are quite different at GL.− 16 m as shown in Fig. 13 (b). The point 'P' in Fig. 13 (b) is considered as an 'error' since the strong earthquake broke the seismometer.

Fig. 14 shows the distribution of maximum value of seismic response analysis at Port Island. At the depth of − 16 m, second peak acceleration is 376.8 (gal) with maximum peak as 564.9 (gal) at the point P in Fig. 13. The alluvial clay layer is located at GL.− 19 m∼ − 27 m, and the viscoelastic-viscoplastic model shows rapid decrease of maximum acceleration in the clay layer, see Fig. 14 (a).

Maximum displacements by two approaches are 66.2 cm and 76.1 cm respectively, at the ground surface in Fig. 14 (b). Reported maximum lateral displacements is 5.1 m large at the waterfront, and decreased with distance inland, 3∼ 40 cm, (Kobe City Development Bureau, 1995). Results by models almost agree with the reported results. Figs. 14 (c) shows shear strain distributions with depth. Because of liquefaction, large shear strains are generated at sand layer (GL.− 5 m∼ − 14 m) while shear strain in the clay layer is around 1 % of strain. Strain developed beneath and above sand layers are larger than the strain of clay layer due to viscous flow effects.

Fig. 15 shows pore water pressure ratio profile with depth and the pore water pressure ratio is a measure of liquefaction potential. The zone of high pore water pressure ratio in excess of 95 % is located at GL.− 7 m∼ − 11 m. From the numerical results, it is clear that liquefaction occurred in the reclaimed land at Port Island and not occurred in the sand layer beneath the clay layer at GL. − 27 m∼ − 65 m. In particular, there is no liquefaction at the depth GL.− 16.25 m, and the numerical results by two

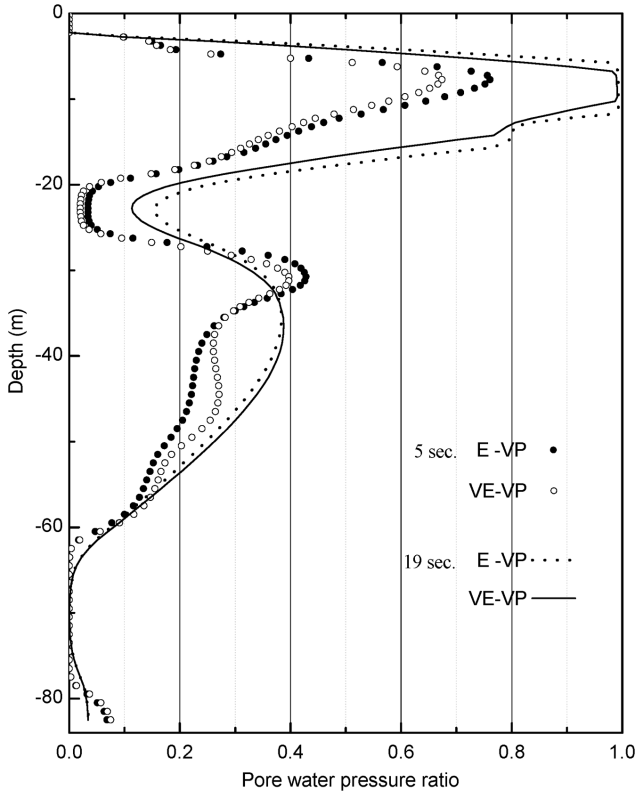

Fig. 15 Excess pore water pressure ratio vs. depth relations at Port Island

models show a big difference in the results of pore water pressure ratio due to clay layer effect.

As for the liquefied layer, several researchers concluded that the alluvial sandy layer beneath the clay layer was liquefied based on numerical simulations. Taguchi et al. (1996) reported that complete liquefaction occurred after a few strong motion cycles in the reclaimed ground. The alluvial sandy layer between GL.－27 m and －33.0 m, which had been thought to be deep enough so as not to liquefy in earthquakes, however, reached the liquefaction state only several seconds in the simulation and they noted that the deep sand layer between GL.－27.0 m and －33.0 m has very low SPT-values.

Sugito et al. (2000) noted that the reclaimed ground at Port Island started to liquefy at around 8 seconds on the time axis. The maximum values of the built up excess pore water pressure at alluvial (dilluvial) sandy layer at Port Island was found to be 80 % of the initial effective overburden pressure. The whole reclaimed layer below sea level of Port Island was liquefied by the strong motion during the earthquake. Arulanandan et al. (2000) reported that the zone of high pore water pressure ratio in excess of 90 % extended in the first 18m from ground surface and at depth of 30 m at Port Island. Evaluated lateral displacements variation with depth in two different directions are 1.0 m in N90E component and 1.5 m in N00E component.

These are quite different results from the present study because there is only liquefaction in the reclaimed ground at GL.－7 m～－11 m. Generally earthquake wave characteristics are related to generation of excess pore water pressure and hysteretic damping of soil.

Moreover, soil layer at GL.－16.25 m did not liquefy and the pore water pressure ratio was around 0.5. Furthermore, reported excess pore water pressure ratio after 14 minutes the main shock at GL.－35 m at Port Island of second phase was 0.49 (Kobe City Development Bureau, 1995). In the present study, evaluated excess pore water pressure ratio at GL.－32.25 m was around 0.4. Therefore, it can be considered that the numerical results are rather less than the recorded one considering a dissipation of pore water pressure.

IV. CONCLUSION

This study has performed liquefaction analysis on the multiple soil layers using a two-dimensional analysis code that applied the viscoelastic-viscoplastic constitutive model of clay and has investigated the role of seismic wave in the behavior of clay. The following conclusions were obtained from the study.

1. The accelerations calculated from the viscoelastic-viscoplastic model were in close agreement with the recorded accelerations on the Port Island down-hole array as well as evaluated lateral displacements by the model were in close agreement with the observed one at Port Island.

2. From the analysis of the amplification characteristics of peak ground motion at Port Island, it was found that the amplification characteristics depend on the softness of the alluvial clay layer under the reclaimed sand.

3. The characteristics of the viscoelastic-viscoplastic model was examined by comparing among the viscoelastic-

viscoplastic model, the elastic-viscoplastic model and obtained records during the mail shock, and then two models gave quite good overall description of the acceleration response with the obtained records in large strain level.

4. This study reveals that the viscoplastic model can describe the characteristics of clay behavior in large strain levels and the viscoelastic-viscoplastic model can explain the clay behavior in wide range of strain level.

This research was supported by Basic Science Research Program through the National Research Foundation of Korea (NRF) funded by the Ministry of Education (NRF-2010-0022456).

REFERENCES

1. Di Benedetto, H., and F. Tatsuoka, 1997. Small strain behavior of geomaterials: Modelling of strain rate effects. *Soils and Foundations* 37(2): 127-138.
2. Hori, M., 1974. Fundamental studies on wave propagation characteristics through soils. Ph. D. Dissertation. Dept. of Civil Engineering. Kyoto Univ. Kyoto. Japan.
3. Kim, Y. S., 2001. A cyclic viscoelastic-viscoplastic constitutive model for clay and Its application to liquefaction analysis. Ph. D. Dissertation, Department of Civil Engineering, Kyoto University, Kyoto, Japan.
4. Kim, Y. S., 2006. Dynamic analysis of sand-clay layered ground considering viscous effect of clay. *Journal of the Korean Society of Agricultural Engineers* 48(7): 45-52 (in Korean).
5. Kim, Y. S., K. Y. Kim, and J. S. Jeon, 2005. Seismic motion amplification characteristics at reclaimed ground. *Journal of the Korean Society of Agricultural Engineers* 47(5): 51-61 (in Korean).
6. Kim, Y. S., and D. W. Lee, 2004. Evaluation technique of seismic performance on agricultural infrastructure. *Journal of the Korean Society of Agricultural Engineers* 46(4): 75-84 (in Korean).
7. Kobe City Development Bureau, 1995. Report on the ground deformation at reclaimed land during the 1995 Hyogoken Nanbu Earthquake. 1-119. KCDB.
8. Kondner, R. L., and M. M. K. Ho, 1965. Viscoelastic response of a cohesive soil in the frequency domain. *Transaction of the Society of Rheology* 9(2): 329-342.
9. Murayama, S. and T. Shibata. 1966. Flow and stress relaxation of clays. *Proc. IUTAM Symp. on Rheology and Soil Mechanics*, 99-129. Grenoble, Kravchenko and Sirieys eds.: Springer-Verlag.
10. Oka, F., A. Yashima, M. Kato, and K. Sekiguchi, 1992. A constitutive model for sand based on the non-linear kinematic hardening rule and its application. *Proc. of 10th World Conf. on Earthquake Engineering*, 2529-2534. 10WCEE, Madrid.
11. Oka, F., A. Yashima, M. Sugito, and Y. Taguchi. 1997. Three dimensional liquefaction analysis of reclaimed island. *Proc. of 7th International Offshore and Polar Engineering Conference*, 665-670. Honolulu.: ISOPE.
12. Oka, F., M. Sugito, A. Yashima, Y. Taguchi, and K. Sekiguchi, 1996. Analysis of strong motion records from the South Hyogo Earthquake of January 17, 1995. *Engineering Geology* 43: 85-106.
13. Oka, F., T. Kodaka, and Y. S. Kim, 2001. A cyclic viscoelastic-viscoplastic model for clay and its application to liquefaction analysis of ground. *Proc. of 10th International Symposium on Computer Methods and Advances in Geomechanics*, 1025-1031. Arizona, Balkema.
14. Taguchi, Y., A. Tateishi, F. Oka, and A. Yashima, 1996. Three-dimensional liquefaction analysis method and array record simulation in Great Hanshin earthquake. Proc. of 11th World Conference on Earthquake Engineering, Acapulco, Sociedad Mexicana de Ingeniera Sismica, A. C. ed., Balkema (CD-Rom), Paper No. 1042.
15. Yashima, A., F. Oka, Y. Taguchi, and A. Tateishi, 1995. Three-dimensional liquefaction analysis considering the compressibility of fluid phase. Proc. of 40th JGS Symposium, 257-264: JGS.